

High-performance dilatometry under extreme conditions

Markus Seidl,¹ Alice Fayter,¹ Josef N. Stern,¹ Katrin Amann-Winkel,^{1,2}
Marion Bauer,^{3,‡} Thomas Loerting^{1,*}

¹ Institut für Physikalische Chemie, Universität Innsbruck,
Innrain 80–82, A-6020 Innsbruck, Austria

² Department of Physics, AlbaNova University Center, Stockholm University,
S-10691 Stockholm, Sweden

³ Institut für Allgemeine, Anorganische und Theoretische Chemie, Universität Innsbruck,
Innrain 80–82, A-6020 Innsbruck, Austria

[‡] Present address: Sandoz GmbH, Biochemiestraße 10, A-6250 Kundl, Austria

* Corresponding author: thomas.loerting@uibk.ac.at, +43 512 507–58019

ABSTRACT

Equations of state describe the pressure-volume-temperature surface of the thermodynamically stable phases of a given material. However, the thermodynamically (most) stable phase might not be observed experimentally due to kinetic reasons. Instead metastable phases could be obtained, which is in fact a very common and technologically important phenomenon. Here we describe how to use a material testing machine from Zwick as a high-performance dilatometer. In conjunction with a custom-made piston cylinder setup it enables the study of phase diagrams as well as metastable phases and instable states, i. e., the experimental representation of equations of state, via both isobaric and isothermal experiments up to pressures of ~ 2 GPa and down to temperatures of ~ 79 K. In particular, we consider amorphous, metastable solid states of water (i. e., amorphous ices) as well as crystalline ice phases to exemplify our apparatus' performance in detail.

I. INTRODUCTION

The equation of state describes how materials change when pressure, temperature and/or volume change. The pioneering work of Boyle, Mariotte, Amontons, Gay and Lussac on gases has allowed to spell out the ideal gas law, $pV = nRT$ (with pressure p , volume V , amount of substance n , temperature T and the ideal gas constant R). This relation is taught to millions of students and exactly describes how an ideal gas reacts to external changes. However, it fails to describe the properties of condensed matter.

In order to facilitate description of condensed matter many modifications to the ideal gas law have been proposed, for instance the van-der-Waals equation of state [1]. By contrast to the ideal gas law this equation is successful in describing how a gas condenses as the temperature is lowered. At this phase transition, from the gaseous to the liquid state, the volume changes discontinuously – a hallmark of a discontinuous, first-order transition [2,3]. However, other common phase transitions such as freezing cannot be described by the van-der-Waals equation. In order to also describe how solids react to external changes more complex equations of state are often employed such as the Murnaghan [4] or Birch-Murnaghan [5] variants. In order to determine such equations of states simultaneous high-precision measurements of pressure, temperature and volume are necessary [6]. In addition to the volume changes of a solid as the pressure is changed described by the Birch-Murnaghan equation of state, phase transitions in the solid also need to be described to understand a material completely. As an example, allotropic, e. g., graphite to diamond, or polymorphic transformations, e. g., from quartz to coesite and stishovite, need to be described. Such phase transitions again involve discontinuous changes in volume and as such are density-driven.

A very common way of representing the equation of state is given by p - T phase diagrams. In these diagrams the thermodynamically most stable phases are shown, whereas kinetically stable, metastable phases are missing. Different phases are separated by phase boundaries in such phase diagrams. One can easily judge from the slope of phase boundaries in the phase diagram whether a phase transition is density-driven or entropy-driven. Entropy-driven phase transformations show a phase boundary parallel to the

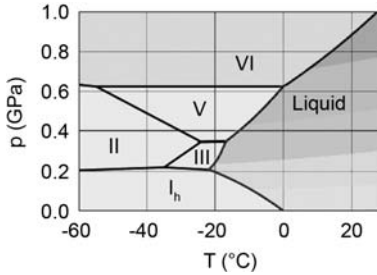


FIG. 1. Phase diagram of the stable phases of water. The thick solid lines are phase boundaries, and Roman numerals denote the stability fields of the respective crystalline polymorphs. Figure is courtesy of Martin Chaplin [8].

pressure axis, whereas density-driven phase transformations show a phase boundary parallel to the temperature axis.

A part of the phase diagram of water is shown in Fig. 1. It is immediately evident that water shows many different crystalline phases of ice (denoted by Roman numerals), and that the phase boundaries between solid phases that share a phase boundary with the liquid are parallel to the temperature axis, implying density-driven phase transformations. Indeed, the density (after recovery to ambient pressure) changes from 0.93 to 1.17 to 1.25 and 1.34 g cm^{-3} when compressing common hexagonal ice (I_h) at -23°C (250 K) to ices III, V and VI, respectively [7].

However, quite often crystalline ice does not even form down to -23°C (250 K) because water remains in the metastable, supercooled state [9]. It is hence also of importance to study phase transitions in the metastable regime, avoiding the transition to the thermodynamically stable form. Research on amorphous water can only be carried out by avoiding the transformation to the crystalline ices indicated in Fig. 1. Also for the description of metastable phases equations of state have to be determined. This can only be done by a very careful control of pressure, temperature and volume and by employing high-precision dilatometry to characterize the metastable materials. Processes that can be monitored using this approach include reversible expansion/contraction of the material, irreversible relaxation by release of stress or spontaneous volume changes incurred upon phase transition, e. g., volume jumps upon crystallization [10].

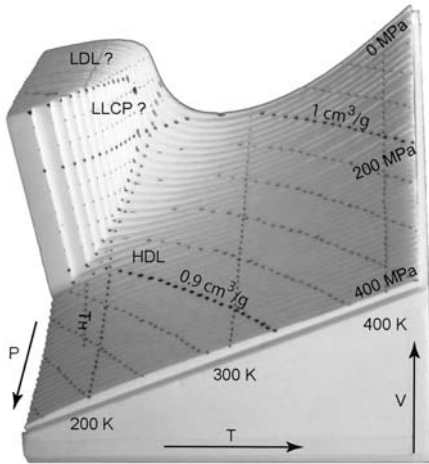


FIG. 2. Three-dimensional model of the p-V-T surface of disordered, i. e., non-crystalline forms of water. T_H is the so-called homogeneous nucleation temperature, LDL and HDL denote the low-density and high-density liquid state, respectively, and LLCP denotes a proposed liquid-liquid critical point [12,13]. Figure is courtesy of Osamu Mishima [14].

Fig. 2 shows a three-dimensional model for the equation of state of metastable water [11]. One of the most interesting aspects seen in this model is the steep cliff below 200 K and at about 200 MPa. This cliff might be indicative of the discontinuous volume change associated with the transition between two different phases of amorphous ice and of liquid water.

The volume jump of an amorphous ice sample indicating this cliff is evident in the series of photographs in Fig. 3. Obviously, it is highly challenging to measure such massive, very sudden changes of volume even at ambient pressure. It is even more challenging to measure such changes at high pressures up to, e. g., 2 GPa and at subzero temperatures as low as $-196\text{ }^\circ\text{C}$ (77 K). Clearly, high-precision dilatometry is required to characterize these phase transitions under such extreme conditions. We could realize such measurements using a material testing machine from Zwick as described in the next section. The uncommon [12], and highly contested [15,16], liquid-liquid phase transition indicated in Fig. 2 might indeed be at

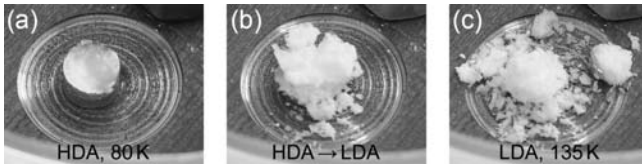


FIG. 3. Visual observation of the transformation of high-density amorphous ice HDA (a) to low-density amorphous ice LDA (c) upon warming at ambient pressure. In the transformation region (b) the sample pops up due to the density difference between the two amorphous polymorphs. Figure adapted from Ref. [17].

the origin of why water is so special [13], so different from other liquids and why only this liquid is considered to be essential for living organisms.

II. EXPERIMENTAL SETUP

A. Material testing machine from Zwick

We utilize a single-screw material testing machine from Zwick, model BZ100/TL3S, for both the preparation of amorphous and crystalline ice polymorphs and the study of phase transitions taking place upon isothermal or isobaric experiments. In conjunction with our custom-made sample environment (a piston cylinder setup with a bore diameter of 8 mm), see Fig. 4, we have a high-pressure apparatus enabling studies up to ~ 2 GPa. In addition, we can work at temperatures as low as ~ 79 K. That is, we have access to the most manifold and most interesting part of the phase diagram, including all kinds of stable and metastable phases of ice [18-20].

The pressure and the sample volume are controlled using Zwick's software TESTXPERT 7.1. The sample volume is controlled via the displacement of pistons, which in turn are moved by the testing machine's mobile crossbar, see Sec. II.B and Fig. 4. The positional reproducibility of the crossbar is ± 5 μm and the spatial resolution of its position is 0.01 μm . At any time during an experiment, the position of the crossbar relative to its

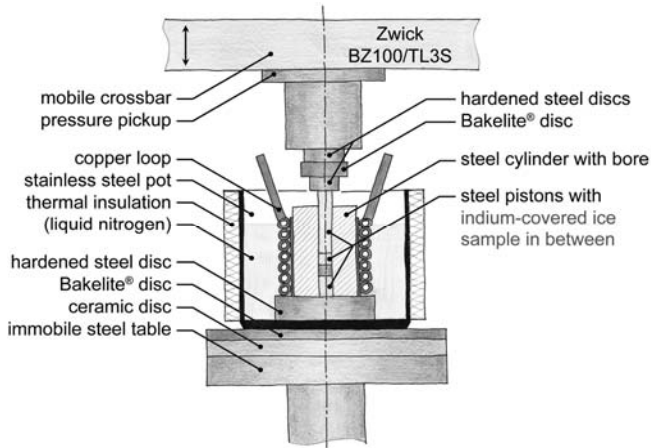


FIG. 4. Schematic drawing of our custom-made high-pressure piston cylinder setup (longitudinal section) placed at the single-screw material testing machine from Zwick (model BZ100/TL3S). In the experiments reported here, a steel cylinder (measuring 50 mm in diameter and 60 mm in height) with a bore of 8 mm and three steel pistons with a total length of 66 mm are used. Furthermore, ice samples are always covered with thin indium foil (~0.3 g). Liquid nitrogen is put into the stainless steel pot in the case that samples should be cooled very fast (“quenching”) and also in the case of isothermal experiments at ~79 K. To accomplish isobaric heating/cooling experiments and isothermal experiments at temperatures >79 K, respectively, liquid nitrogen is pumped through the copper loop enclosing the cylinder. For simplicity, the holes for the Pt-100 sensor used for temperature measurement and the two resistive heaters enabling controlled heating are not drawn.

position at the beginning of the experiment (Δd) as well as the elapsed time (t), the pressure (p) and the temperature (T) are recorded.

Δd reflects changes of the sample’s height (and, thus, changes in the sample’s volume) plus changes of the physical dimensions of all other parts between the mobile crossbar and the immobile steel table. Among these parts, the pistons probably contribute most to Δd via changes in their total length. However, for simplicity we usually call Δd “piston displacement”, being aware that it has to be corrected for the apparatus contribution (see Sec. III.C) to obtain the samples’ contribution only.

B. Custom-made sample environment

The essential heart of our custom-made sample environment illustrated in Fig. 4 is a 60-mm-high steel cylinder with an 8-mm-wide bore which is closed with a 20-mm-long steel piston at the bottom end. It is placed on a hardened steel disc inside a stainless steel pot (a commercially available cooking pot with a solid bottom) which is thermally insulated. The pot itself is placed on discs made of Bakelite[®] and ceramics which rest on the immobile steel table of the material testing machine.

The whole setup can be cooled quickly to a temperature of ~ 79 K by filling the pot with liquid nitrogen. For slower and better controlled cooling or for isothermal experiments at $T > 79$ K, a copper loop enclosing the cylinder is mounted in the beginning of the experiment. Liquid nitrogen is then pumped through the copper loop, where the flow can be adapted manually, enabling, e. g., different cooling rates. In any case, the setup is cooled to ~ 79 K before inserting the ice sample into the cylinder's bore. During cooling the top end of the bore is covered with, e. g., a steel disc to avoid condensation of ice from moist air inside the bore.

Once that the setup has reached ~ 79 K the ice sample (for the preparation of the sample see below) followed by two steel pistons with a length of 8 mm and 38 mm, respectively, are put into the bore. The long piston sticks out from the cylinder by ~ 1 cm so that the further setting consisting of two hardened steel discs and a Bakelite[®] disc in between can then be compiled on the top of the piston. Now the mobile crossbar is moved downward close to the most upper steel disc. After making sure that the whole setup is aligned to the vertical axis, the crossbar is moved further downward to get in contact with the steel disc and to build up a pre-force of 500–1000 N on the sample. The setup is now built up completely; the further progress then depends on the actual experiment to be carried out.

We typically start with hexagonal ice I_h which is produced by pipetting liquid water into a pre-cooled cylindrical container made out of indium [21,22]. The size of the container and, thus, its mass depend on the sample volume. In all studies reported here, see Sec. III.A and III.B, 300 μl water are used, requiring thin indium foil with a mass of ~ 0.3 g for the preparation of the container. Accordingly, our studies on the apparatus behavior

(in which only indium but no ice are inserted into the cylinder's bore), see Sec. III.C, are carried out using the same amount of indium. The indium acts as a low-temperature lubricant reducing friction between the ice sample and the walls of the steel cylinder. Its necessity has been demonstrated before, showing that pressure drops may appear when the ice sample is not covered with indium. These pressure drops are considered to generate shock waves which cause transient local heating of local spots in the sample which in turn may enable (unwanted) phase transitions to take place [22].

The temperature is measured using a Pt-100 sensor which is inserted firmly in a hole of the steel cylinder. Similarly, two resistive heaters are placed in two other holes. This arrangement in conjunction with the cooling loop enclosing the cylinder enables heating/cooling experiments following a well-defined temperature program. In fact, we simultaneously cool and heat the cylinder to gain the desired temperature. Here, the basic temperature control is accomplished using a LABVIEW program (a proportional-integral-derivative controller). This program regulates the power of the resistive heaters to gain, e. g., a certain heating rate, while the flow of liquid nitrogen through the copper loop is usually adapted manually.

Since we measure the temperature of the steel cylinder somewhere between its curved surface and its central bore, there generally is a difference between the actual temperature of the sample (sitting in the bore) and the temperature readout. Of course, the extent of this difference depends both on the type of experiment, i. e., on the realized temperature program, and on the physical processes taking place inside the sample, e. g., structural relaxation or thermodynamic phase transitions. For a very similar setup as described here, Salzmann *et al.* estimated that for slow heating the samples' temperature differs from the temperature readout by ± 3 K [23]. In the case of isothermal experiments the difference between these temperatures can be assumed to be zero as long as significant friction is avoided and phase transitions being associated with the release of latent heat do not take place. In fact, if indium is used to cover the ice sample, the friction in our setup is very low [24]. Furthermore, the pressure-induced phase transition between ice I_h and high-pressure ice polymorphs at ~ 170 K and the very high compression rate of ~ 2 GPa/min leads to sample heating of only 5 K (as mo-

nitored by a K-type thermocouple frozen directly within the ice sample) [25].

Due to the low friction the real pressure which acts on the sample can be considered to be equal to the nominal pressure in good approximation. Using a setup being very similar to ours Salzmann *et al.* calibrated the pressure by following the pressure-induced phase transition between ice V and ice VI which takes place at ~ 0.7 GPa. They found that in this pressure region the real pressure and the nominal pressure differ by less than 0.04 GPa [26].

III. DILATOMETRY AT HIGH PRESSURE AND LOW TEMPERATURE

As described in the previous section, our apparatus allows studies under extreme temperature-pressure conditions. In the following we demonstrate its performance by showing details of experiments reported in two of our most recent studies on the so-called expanded high-density amorphous ice (eHDA) [10,27].

Fig. 5 illustrates the preparation of eHDA from hexagonal ice I_h via multiple steps. The preparation of the (indium-covered) ice I_h sample itself has already been described in Sec. II.B. First the ice I_h sample is isothermally compressed to 1.6 GPa at ~ 79 K and at a rate of 0.10 GPa/min (step ①). During this step ice I_h transforms to so-called unannealed high-density amorphous ice (uHDA) [21]. The sample is then decompressed to 1.1 GPa at ~ 79 K, applying a rate of 0.10 GPa/min, and subsequently heated isobarically to 160 K at a rate of 2 K/min (step ②). This high-pressure annealing leads to the formation of very high-density amorphous ice (VHDA) [28]. Afterwards, the sample is brought to 140 K applying a cooling rate of 2 K/min, followed by isothermal decompression to 0.20 GPa at a rate of 0.02 GPa/min (step ③). In this step VHDA transforms to the desired final state, i. e., eHDA [29-31]. Immediately after having reached the final pressure of 0.20 GPa, the sample is rapidly cooled (i. e., “quenched”) to ~ 79 K while the pressure is kept constant (step ④).

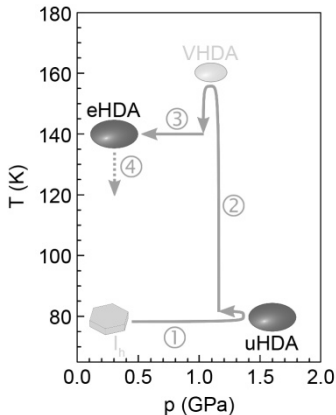


FIG. 5. Scheme illustrating the particular steps to prepare eHDA from ice I_h . In step ① ice I_h is transformed to uHDA via pressure-induced amorphization at ~ 79 K. Subsequent high-pressure annealing at 1.1 GPa, step ②, results in VHDA which is then transformed to eHDA via isothermal decomposition at ~ 140 K, step ③. Finally eHDA is quench-recovered to ~ 79 K (step ④). Amorphous ices are represented by ellipses where their size indicates the molar volume of the respective phase. Figure adapted with changes from Ref. [10].

TABLE I. List of the pressures applied in particular experiments. The *rounded* pressure is used to describe the experiments in the text. However, the *nominal* pressure is the one that has actually been applied. It is given by the applied force divided by the cross section of the steel cylinder's bore. The diameter of the bore is 8 mm and considered to be independent of the actual temperature and pressure.

rounded pressure (GPa)	applied force (N)	nominal pressure (GPa)
0.001	50	0.0010
0.10	5000	0.0995
0.20	10000	0.1989
0.30	15000	0.2984
0.50	25000	0.4974
0.70	35000	0.6963
1.1	55000	1.0942
1.6	80000	1.5915

We utilize x-ray powder diffraction as a standard method to characterize the sample at the end of the experiment. Even though the amorphous ices do not show sharp Bragg reflexes due to the lack of long-range order, they exhibit a broad halo peak with a maximum at a position characteristic for the respective phase [28,29,31,32]. Of course, there are many other methods probing structural, dynamic or thermodynamic properties, elucidating the differences between the distinct amorphous states of water [18].

Please note that we use rounded pressure values throughout this article. In Table I we show these values along with the forces that have actually been applied as well as the nominal pressures following from them.

A. Isothermal experiments

We now discuss the temporal evolution of pressure (p), temperature (T) and piston displacement (Δd) for the isothermal steps in the preparation of eHDA, i. e., step ① and step ③ illustrated in Fig. 5.

The top graphs in the left (step ①) and right panel (step ③) of Fig. 6 show the pressure program as operated by TESTXPERT 7.1, while the middle graphs show the temperature throughout the experiment. It can easily be seen that the temperature is kept constant with an accuracy of a few tenth of a Kelvin. While the cylinder containing the sample is cooled by simply immersing it in liquid nitrogen in step ①, it is simultaneously cooled and heated in step ③ to gain a temperature of 140 K. In the latter case, the LABVIEW program regulates the power of the resistive heaters, while the flow of liquid nitrogen through the copper loop can easily be adapted manually, at least with some experience. However, we have to point out that the thermal bath provided by liquid nitrogen is much more stable than the system's control via balancing simultaneous heating and cooling. That is, isothermal experiments resting on the latter might cause issues if significant latent heat were suddenly released.

As described in Sec. II, the sample's height (and, thus, the sample volume) is controlled via the displacement of the pistons (Δd) which in turn are moved by the testing machine's mobile crossbar. That is, our apparatus represents a dilatometer which enables us to detect physical processes tak-

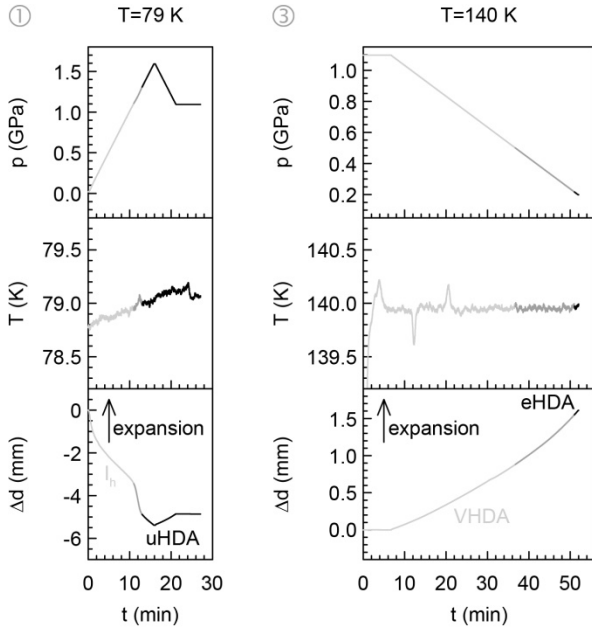


FIG. 6. Physical properties recorded during the isothermal steps depicted in Fig. 5. In the left panel the formation of uHDA via pressure-induced amorphization of ice I_h at ~ 79 K, applying a rate of 0.10 GPa/min, is followed (Step ① in Fig. 5). In the right panel the transformation of VHDA to eHDA by isothermal decompression at ~ 140 K, applying a rate of 0.02 GPa/min, is followed (Step ③ in Fig. 5). The piston displacement Δd reflects changes of the sample's height (and, thus, the sample's volume) plus changes of the physical dimensions of all other parts between the mobile cross-bar and the immobile steel table; for details on the apparatus' contribution see Sec. III.C in the main text. In each panel, curves are light gray (black) to indicate presence of the starting material (final material), while the transformation region between the starting and the final material is indicated by an intermediate grayscale.

ing place in the sample in the case that they are associated with changes in the sample's density. In the examples shown in Fig. 6, a rather sharp, i. e., discontinuous transition with respect to the piston displacement Δd takes place in step ① while a continuous transition takes place in step ③: After the compaction of hexagonal ice I_h upon compression at ~ 79 K (bottom

graph in the left panel, light gray part of the curve), a step in Δd around 12 min or at a pressure around 1.2 GPa (gray part of the curve) indicates its amorphization to uHDA (black part of the curve) [21]. At this temperature, uHDA does not transform back to crystalline ice or to another amorphous phase upon decompression. In comparison, during the decompression of VHDA at ~ 140 K (bottom graph in the right panel, light gray part of the curve) its transformation to eHDA (black part of the curve) is not accompanied by a step in Δd . Instead, a rather large transition region starting around 37 min or at a pressure around 0.5 GPa (gray part of the curve) has been found by following structural properties [29] as well as kinetic properties [31].

B. Isobaric experiments

Very recently, we have studied eHDA's stability against phase transformations upon isobaric heating in a broad pressure range [10,33]. Furthermore, we have investigated the relaxation processes taking place in the sample just prior to the start of any phase transformation [27]. In both cases we have utilized a combination of our material testing machine as dilatometer and *ex situ* powder x-ray diffraction for the structural characterization of the recovered samples. In this section we show the temporal evolution of pressure (p), temperature (T) and piston displacement (Δd) or volume change (ΔV) obtained in these experiments (see Figs. 7–9) to discuss the performance of our apparatus in the case of isobaric heating/cooling.

Upon isobaric heating at pressures below ~ 0.1 GPa, HDA undergoes an amorphous-amorphous transition to low-density amorphous ice (LDA), see Fig. 3. Since uHDA and eHDA have been obtained via different routes (see Fig. 5) and since they have been found to differ in the degree of internal stress [34], thermal stability [10,31,33,34] and microscopic structure [10,33] it is meaningful to indicate whether LDA is formed from uHDA or eHDA. For this reason, we distinguish LDA_I (obtained from uHDA) and LDA_{II} (obtained from eHDA). Analogous to the two forms of HDA, also the two types of LDA differ in, e. g., thermal stability [10,35] and structural details [36].

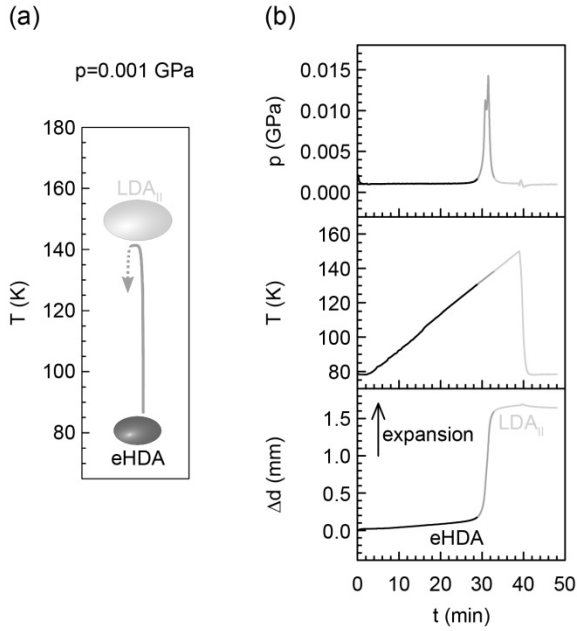


FIG. 7. Transformation of eHDA to LDA_{II} upon isobaric heating at 0.001 GPa. (a) Schematic representation of this amorphous-amorphous transition. Amorphous ices are represented by ellipses where their size indicates the molar volume of the respective phase. Figure adapted with changes from Ref. [10]. (b) Physical properties recorded during the transformation. In the example shown here controlled heating at a rate of 2 K/min has been applied, while cooling has been achieved by quenching with liquid nitrogen at the maximum temperature. The piston displacement Δd reflects changes of the sample's height (and, thus, the sample's volume) plus changes of the physical dimensions of all other parts between the mobile crossbar and the immobile steel table; for details on the apparatus' contribution see Sec. III.C in the main text. The corresponding volume change ΔV is plotted as a function of temperature in Fig. SM1(b1) in the Supplemental Material of Ref. [10] (heating only). Curves are black (light gray) to indicate presence of eHDA (LDA_{II}), while the transformation region between eHDA and LDA_{II} is indicated by an intermediate grayscale.

The schematic in Fig. 7(a) illustrates the transformation $\text{eHDA} \rightarrow \text{LDA}_{\text{II}}$ at 0.001 GPa, while the physical properties measured during the experiment

are plotted in Fig. 7(b). The piston displacement Δd shown in the bottom graph exhibits a large and sharp step around 31 min or around 135 K, clearly indicating the first order-like/discontinuous transition (gray part of the curve) between eHDA (black part of the curve) and LDA_{II} (light gray part of the curve). At 0.001 GPa, LDA_{II} does not transform back to eHDA upon subsequent cooling. The top graph in Fig. 7(b) shows the pressure program throughout the experiment as operated by TESTXPERT 7.1. While the pressure is constant with high accuracy for heating eHDA (low-temperature end, black part of the curve) and LDA_{II} (high-temperature end, light gray part of the curve), a pronounced increase in pressure (gray part of the curve) reflects the sudden change in the sample's density, just as the piston displacement Δd does. That is, the transformation of eHDA to LDA_{II} develops so fast that the automated material testing machine cannot keep the pressure constant. However, the phase behavior is governed by the pressure at the very beginning of the transformation so that the pressure increase (developing during the transformation) is not expected to have a qualitative impact on, e. g., the transition temperature. The middle graph in Fig. 7(b) shows the temperature program throughout the experiment as operated by our LABVIEW program. It is evident that the heating rate, i. e., the slope of the T(t) curve is rather constant. Similar to isothermal experiments at temperatures above 79 K, the flow of liquid nitrogen through the copper loop has to be adapted manually in the very beginning. Usually there's no need to further adjust the flow during the heating run, at least up to a maximum temperature of 210 K.

From the phenomenological point of view, similar results are found for the crystallization of eHDA upon isobaric heating at 0.20 GPa, see Fig. 8. Again, the transformation process is associated with a decrease in the sample's density as evident from the evolution of the piston displacement $\Delta d(t)$ and pressure $p(t)$, see Fig. 8(b). However, at this pressure the sample crystallizes to ice IX. This crystallization is much faster (taking only a few seconds) than the amorphous-amorphous transition shown in Fig. 7. In fact, in the pressure evolution $p(t)$ it appears just as a spike at ~ 40 min (where $T \sim 150$ K). After reaching the maximum temperature the ice IX sample is cooled slowly (with 2 K/min) to ~ 115 K and subsequently quenched to ~ 79 K, see the middle part of Fig. 8(b). It can clearly be seen

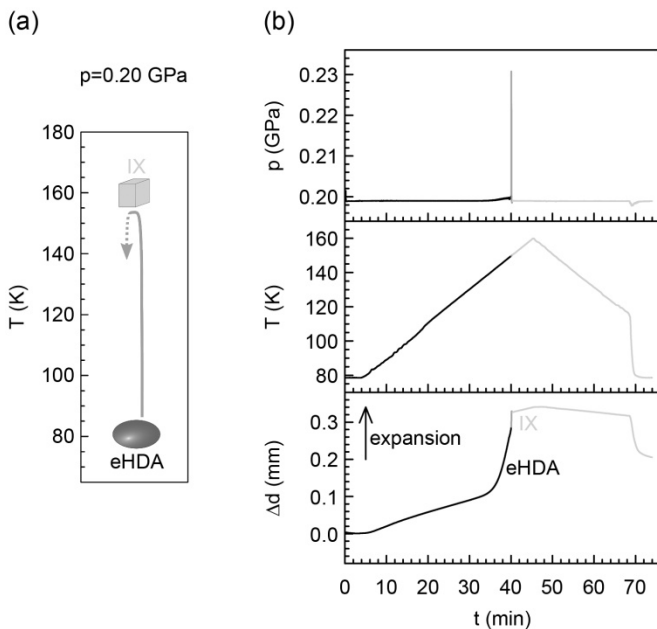


FIG. 8. Transformation of eHDA to ice IX upon isobaric heating at 0.20 GPa. (a) Schematic representation of this crystallization process. Figure adapted with changes from Ref. [33]. (b) Physical properties recorded during the transformation. In the example shown here controlled heating/cooling at a rate of 2 K/min has been applied. Upon reaching ~ 115 K during cooling, the sample has been quenched with liquid nitrogen. The piston displacement Δd reflects changes of the sample's height (and, thus, the sample's volume) plus changes of the physical dimensions of all other parts between the mobile crossbar and the immobile steel table; for details on the apparatus' contribution see Sec. III.C in the main text. The corresponding volume change ΔV is plotted as a function of temperature in Fig. SM2(d1) in the Supplemental Material of Ref. [10] (heating only). Curves are black (light gray) to indicate presence of eHDA (ice IX), while the transformation region between eHDA and ice IX is indicated by an intermediate grayscale.

that our experimental setup is also perfectly suitable for controlled cooling (at least down to ~ 115 K), even though in this case the desired temperature program is realized by continuously adapting the nitrogen flow manually.

We want to emphasize that the pronounced change in the slope of the Δd curve around 36 min (where $T \sim 140$ K), see the bottom part of Fig. 8(b), does not reflect the beginning of crystallization. *Ex situ* powder diffraction shows that the sample is pure eHDA up to the sudden jump at ~ 40 min (where $T \sim 150$ K), see Fig. SM3(f) in the Supplemental Material of Ref [10]. That is, the sample's expansion in this range (i. e., below the crystallization temperature of ~ 150 K) is solely caused by structural relaxation processes.

In general, both irreversible and reversible relaxation may take place. The former would be observed if the sample was far from equilibrium. In fact, eHDA as prepared in the present study is close to an equilibrated state [31], but due to finite transformation kinetics in the final step of its preparation (VHDA \rightarrow eHDA, step ③ in Fig. 5) and due to the immediate quench recovery upon reaching 0.20 GPa it continues to relax significantly [33]. However, we have shown that consecutive heating/cooling cycles (with a maximum temperature of 144 K) performed at 0.20 GPa result in a very well relaxed sample which does not show irreversible relaxation any longer [27]. Nevertheless, there remains a reversible relaxation process which we discuss in detail now.

From a theoretical point of view amorphous ices are most interesting because of their structural similarity with the liquid state. While crystals show long-range order of the molecules (or atoms), liquids and amorphous solids lack this kind of order [37]. Instead, they only show short-range (or local) order of the molecules. If liquids are cooled fast enough below their melting point, crystallization does not have time enough to take place. One then ends up with a glassy solid [38,39]: The molecular motions progressively slow down upon cooling and become arrested with respect to the experimental time scale given by the cooling rate. Hence, equilibrium cannot be restored any longer. The corresponding temperature region is characterized by the so-called glass transition temperature T_g . The material under scrutiny is a liquid (i. e., in an equilibrium state) above T_g , while it is a glass (which is a non-equilibrium state by definition) below T_g . Amorphous ices exhibit glass-like (but also crystal-like) properties even though most of them are not prepared from liquid water [20,40,41]. Thus, it is discussed controversially whether or not they are glasses or, in other words, low-tem-

perature proxies of liquid water. If the *distinct* amorphous ices indeed were glasses, there would also be *distinct* liquid states of water – a phenomenon called liquid polymorphism (or polyamorphism) [42]. In fact, some computer simulation studies provide support for the existence of different liquid states of water [43]. Based on this insight a scenario capable to explain many of water’s anomalous properties has been established [13,43]. However, on the experimental side there is an ongoing debate on whether or not LDA and HDA are related to liquid states of water. Beside recent skepticism [44], it is commonly accepted that LDA turns into a corresponding liquid state upon heating, while such a relation has remained completely unclear in the case of HDA for a long time [45].

Utilizing our material testing machine as high-performance dilatometer we made significant progress towards the clarification of HDA’s nature very recently [27]. As discussed below it turns out that the thermal expansion behavior of eHDA indeed exhibits a feature characteristic for a glass transition. The method is based on the fact that a glassy state and its corresponding liquid state generally show different thermal expansion coefficients. Accordingly, the volume-temperature curve $V(T)$ changes its slope in a rather small temperature region around T_g [38]. Instead of measuring the absolute volume one may also consider the volume relative to a certain reference point, e.g., the volume in the beginning of the experiment. That is, the volume change $\Delta V(T)$ as obtained from the piston displacement $\Delta d(T)$ by simply multiplying it with the area of the bore’s cross section is a suitable property to detect glass transitions. We benchmarked this method using glycerol [46] because it is a well-studied, good glass former which means that the whole supercooled liquid regime down to the glass transition region is easily accessible without crystallization taking place. In contrast, water is a bad glass former and eHDA crystallizes very rapidly at ~ 150 K at 0.20 GPa. For this reason we have expected to observe only the beginning of the glass transition region (if at all). Therefore, our ultimate aim has been to determine the onset glass transition temperature $T_{g, \text{onset}}$.

As evident from Fig. 9(a) we find that eHDA’s volume change $\Delta V(T)$ is linear at the low-temperature end, while its slope increases between 135 K and 140 K, depending on the actual number of the heating run of consecutive isobaric heating/cooling cycles. The deviation from the low-tempera-

ture linearity decreases from the first to the fifth heating run, indicating irreversible structural relaxation towards a stress-free state of lower energy. However, the $\Delta V(T)$ curves of the fifth and sixth heating run reveal a reversible relaxation process since the deviation from linearity starts at the same temperature (dashed vertical line) and since its extent is very similar in both runs. As discussed above, such a change in the slope of $\Delta V(T)$ indicates the transition from a glassy state to its corresponding liquid state. Hence, we indeed find a signature for eHDA's transition to a high-density, ultraviscous liquid. Upon cooling this liquid again vitrifies, freezing in the structure present above $T_{g, \text{onset}}$ and leading to the same deviation from linearity in the $\Delta V(T)$ curve in the subsequent heating run. That is, while the release of significant internal stress discussed above is irreversible, the non-equilibrium feature of well-relaxed eHDA observed here is reversible.

A heating experiment on crystalline ice confirms that the observed feature really reflects eHDA's behavior rather than the one of the apparatus, because in the case of a crystalline sample linear expansion is observed over the whole temperature range, see Fig. 9. Furthermore, experiments without ice directly reflecting the apparatus' behavior do not show a change in the slope of $\Delta d(T)$, as becomes evident by comparison of the bottom part of Fig. 9(b) (eHDA) and the bottom part of Fig. 10(c) (apparatus only).

Details on the temporal evolution of several physical properties upon isobaric heating of eHDA (fifth and sixth cycle) and ice IX are shown in Fig. 9(b). For all three cases the middle graph shows a small increase in the heating rate since a change in the property $T-T_{\text{linear}}$ indicates a deviation from a linear temperature program. It could be caused by a subtle compaction of the respective ice sample since a change in the piston displacement Δd is evident, too (see the bottom graph for non-linear changes in Δd). Such a compaction may be associated with the release of heat due to some friction, causing a slightly higher heating rate. However, at least some of the experiments without ice show a similar feature in $\Delta d-\Delta d_{\text{linear}}$ and $T-T_{\text{linear}}$, see the bottom part of Fig. 10(c). Therefore, this feature could also be due to some friction between the pistons and the steel cylinder.

The curves for eHDA shown in Fig. 9(b) are drawn up to the point where any of the evaluated properties just shows changes due to the cooling process which starts shortly prior reaching the maximum temperature.

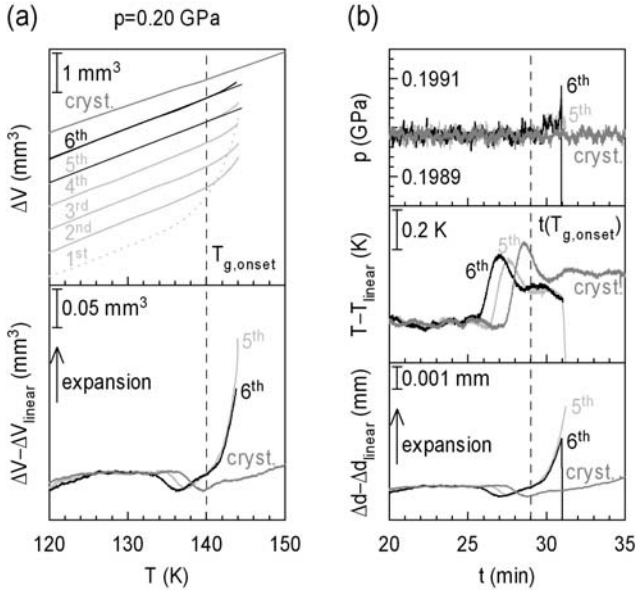


FIG. 9. Experiments to determine the glass transition temperature T_g of eHDA at 0.20 GPa. (a) By following the volume change $\Delta V(T)$, top part of panel (a) (curves are vertically shifted for clarity), consecutive isobaric heating/cooling cycles (heating/cooling rate: 2 K/min, maximum temperature: 144 K; only heating runs are shown) reveal a *reversible* deviation from linear expansion behavior at a certain temperature (dashed vertical line). This temperature, $T_{g, \text{onset}}$, is interpreted to indicate the onset of the glass transition. In comparison, the volume change upon heating *crystalline* ice (ice IX) shows linear expansion behavior over the whole temperature range considered here (curve labeled “cryst.”). In the case of the 5th and 6th heating run, a linear function obtained by fitting the data in the range 125–133 K illustrates the linear expansion at the low-temperature end (solid black lines). ΔV is calculated from the piston displacement Δd by multiplying with the area of the bore’s cross section, assuming a temperature-independent bore diameter. A magnified view on selected curves is presented in the bottom part of panel (a). The data have been obtained by subtracting linear functions ($= \Delta V_{\text{linear}}$, see the black lines in the top panel) from the original data. That is, non-constant segments of the $(\Delta V - \Delta V_{\text{linear}})$ curves indicate a deviation from the linear expansion at the low-temperature end. Figure adapted with changes from Ref. [27]. (b) A detailed view on the physical properties recorded during isobaric heating of eHDA (5th and 6th cycle only) and ice IX (curves labeled “cryst.”), respectively.

After the fifth heating run slow cooling was realized, while after the sixth heating run the sample was quickly cooled by quenching with liquid nitrogen. While in the former case the cooling process first becomes evident in the temperature evolution (see the steep part at the end of the respective curve in the middle panel) it can be recognized at first in the evolution of the pressure and the piston displacement in the latter case (see the steep part at the end of the respective curve in the top and in the bottom panel).

At the end of this section we want to point out that the performance of our material testing machine and our sample environment is remarkable. Without the high spatial resolution of the machine's crossbar and the high quality of the applied temperature program it would not have been possible to detect the subtle volume changes associated with eHDA's glass transition.



FIG. 9. (*Continued*) In the eHDA runs shown here controlled heating at a rate of 2 K/min (5th and 6th cycle) and controlled cooling at the same rate (5th cycle) or quenching with liquid nitrogen at the maximum temperature (6th cycle) have been applied. The curves are shown up to the point where any property just shows changes due to the cooling process (see main text). The middle part of panel (b) shows $T-T_{\text{linear}}$ where $T(t)$ is the actual temperature and $T_{\text{linear}}(t)$ is a linear function obtained by fitting the $T(t)$ data in the range 20–25 min. Thus, at non-constant segments of the curves a deviation from the ideal temperature program (defined by a heating rate of 2.0 K/min) has been obtained. The bottom part of panel (b) shows $\Delta d-\Delta d_{\text{linear}}$ where $\Delta d(t)$ is the actual piston displacement and $\Delta d_{\text{linear}}(t)$ is a linear function obtained analogously to ΔV_{linear} (see above). That is, non-constant segments of the $(\Delta d-\Delta d_{\text{linear}})$ curves indicate a deviation from the linear expansion at the low-temperature end. The dashed vertical line marked “ $t(\Gamma_{g, \text{onset}})$ ” indicates the position on the time axis at which $T_{g, \text{onset}}$ is reached; all curves have been shifted along the time axis according to $t(\Gamma_{g, \text{onset}})=29$ min. In all cases, the temperature at 20 min is 122 K, i. e., approximately the same temperature range as shown in panel (a) is covered. Both ΔV and Δd reflect changes of the sample's height (and, thus, the sample's volume) plus changes of the physical dimensions of all other parts between the mobile crossbar and the immobile steel table; for details on the apparatus' contribution see Sec. III.C in the main text.

C. Apparatus correction

The piston displacement Δd shown in Fig. 6 to Fig. 8 as well as the volume change ΔV shown in the top part of Fig. 9(a) reflect changes of the sample's height plus changes of the physical dimensions of all other parts between the mobile crossbar and the immobile steel table. However, in some

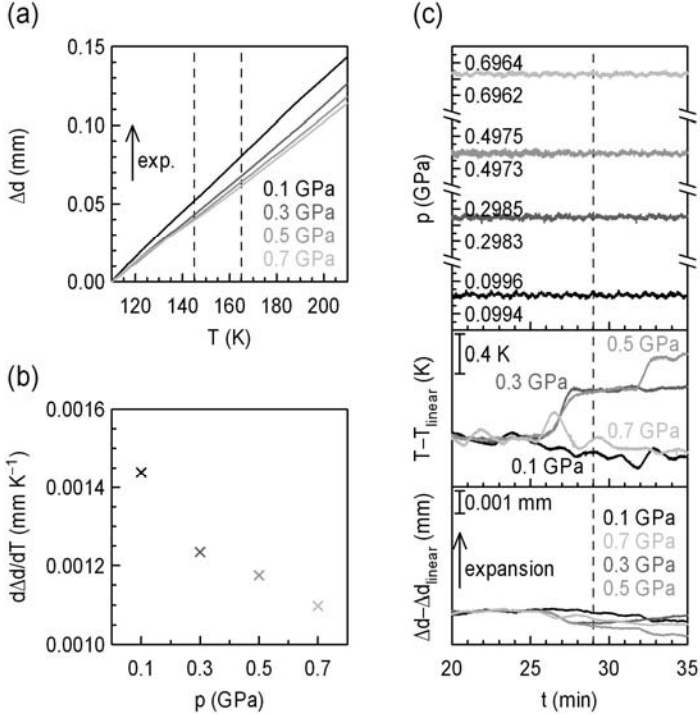


FIG. 10. Apparatus behavior upon isobaric heating in the pressure range from 0.1 to 0.7 GPa. (a) Piston displacement Δd as a function of temperature as obtained by putting ~ 0.3 g indium but no ice into the steel cylinder. It is evident that, for a given pressure, the apparatus exhibits a nearly linear $\Delta d(T)$. (b) Slopes of linear functions obtained by fitting the $\Delta d(T)$ data shown in panel (a) in the range 145–165 K [vertical dashed lines in panel (a)]. (c) A more detailed view on the physical properties of the

cases it is meaningful to plot the sample's contribution only. For example, analysis of irreversible structural relaxation processes might require Δd or ΔV to be corrected for the apparatus contribution to see whether expansion or densification is associated with the relaxation (see Fig. 6 and Sec. III.A in Ref. [33]).

In the case of isobaric heating experiments it is straightforward to correct the raw data for the apparatus' contribution. Fig. 10(a) shows the piston displacement $\Delta d(T)$ as obtained upon isobaric heating of solely ~ 0.3 g indium at four different pressures from 0.1 to 0.7 GPa. From the almost linear curves it follows that a straight line accounts for the apparatus' behavior in good approximation. By fitting the $\Delta d(T)$ data in the range 145–165 K (vertical dashed lines) one obtains linear functions being very suitable for the correction of raw data; Fig. 10(b) reports the slopes of these linear functions. (The performance of our apparatus is again illustrated in Fig. 10(c), now showing the temporal evolution of several physical properties obtained in the experiments on indium only.)

Since we have primarily focused on isobaric experiments in this article, we refrain from a detailed discussion of the apparatus contribution to Δd in isothermal compression/decompression experiments here. However, we



FIG. 10. (*Continued*) experiments already shown in panel (a). The middle part of panel (c) shows $T - T_{\text{linear}}$ where $T(t)$ is the actual temperature and $T_{\text{linear}}(t)$ is a linear function obtained by fitting the $T(t)$ data in the range 20–25 min. Thus, at non-constant segments of the curves a deviation from the ideal temperature program (defined by a heating rate with a value between 1.9 and 2.0 K/min) has been obtained. The bottom part of panel (c) shows $\Delta d - \Delta d_{\text{linear}}$ where $\Delta d(t)$ is the actual piston displacement and $\Delta d_{\text{linear}}(t)$ is a linear function obtained analogously to ΔV_{linear} shown in Fig. 9 (see the caption of Fig. 9). That is, non-constant segments of the $(\Delta d - \Delta d_{\text{linear}})$ curves indicate a deviation from the linear expansion at the low-temperature end. The dashed vertical line indicates the position on the time axis at which $T_{\text{gs, onset}}$ of eHDA at 0.20 GPa [see Fig. 9(a)] is reached; all curves have been shifted along the time axis to fulfill the condition $t(T_{\text{gs, onset}}) = 29$ min. In all cases, the temperature at 20 min (35 min) is 122 K (152 K), i. e., only a part of the temperature range covered in panel (a) is considered here. Δd reflects changes of the indium's height and, presumably to a much larger extent (cf. Ref. [47]), changes of the physical dimensions of all parts between the mobile crossbar and the immobile steel table.

have already reported such experiments in earlier work where Δd was corrected for the apparatus' contribution to allow the calculation of the pressure-dependent sample density [47]. We have shown that in this case the apparatus' contribution depends on the temperature and that there is a hysteresis between compression and subsequent decompression where its extent depends on the maximum pressure.

IV. CONCLUSIONS

To conclude, our high-pressure apparatus allows us to prepare both amorphous and crystalline ice polymorphs and to study both thermodynamically and kinetically controlled transitions between these phases.

We are able to apply a maximum pressure of ~ 2 GPa, which is much larger than the pressure at which ice is found in the deepest glaciers or ice sheets on Earth. In order to transform ice to one of its high-pressure forms, namely ice II, an ice sheet of at least 10 km thickness would be required. For this reason, one always finds crystalline ice in its low-pressure form (i. e., hexagonal ice I_h) on Earth. The only exception might be the suspected occurrence of high-pressure ice phases (particularly ice VI and ice VII) in subduction zones [48]. In contrast, in outer space high-pressure ice phases exist. For instance, the largest moon in the Solar System, Ganymede, is covered with a well-separated icy mantle of 900 km thickness and presumably consists of layers of ice I, ice II, ice V and ice VI as one progresses into its interior [49]. The majority of all water in outer space, though, mainly exists in the low-density amorphous state, especially as a component enveloping interstellar dust. It is believed to play a key role in a number of processes, e. g., in promoting chemical reactions or even in the formation of planets [50].

In this astronomical context and beyond, it is of highest interest whether or not amorphous ice phases could soften and finally form liquid phases, following a theoretical suggestion [12,13,43]. Due to fast crystallization kinetics at temperatures above ~ 150 K one has to search for such a transition at rather low temperatures. Utilizing the high performance of our

material testing machine from Zwick we have indeed found signatures for the liquefaction of two amorphous ice phases very recently [27]. Our observation indicates the existence of two distinct liquid states of water, thus supporting two-liquid theories of water [12,13,51]. With this experimental progress we significantly move toward a comprehensive understanding of the anomalous properties of water.

ACKNOWLEDGMENTS

We thank Philip Handle for the initial design of the symbols used in Fig. 5, Fig. 7(a) and Fig. 8(a). Support by the European Research Council ERC (Starting Grant SULIWA to T.L.), the Austrian Science Fund FWF (START Award Y391 to T.L., Hertha-Firnberg fellowship to K. A.-W. and French-Austrian bilateral project I1392) and the Austrian Academy of Sciences (DOC fellowship to M.S.) is gratefully acknowledged. Furthermore, M.S. is very grateful to the Zwick GmbH & Co. KG for honoring his work with the *Paul Roell Medal*.

REFERENCES

- [1] J. D. van der Waals, *Over de Continuïteit van den Gas- en Vloeistofstoestand*. Ph. D. thesis, Leiden University, 1873.
- [2] P. Ehrenfest, *Proceedings Royal Acad. Amsterdam* 36, 153–157 (1933).
- [3] G. Jaeger, *Arch. Hist. Exact Sci.* 53, 51–81 (1998).
- [4] F. D. Murnaghan, *Proc. Natl. Acad. Sci. U. S. A.* 30, 244–247 (1944).
- [5] F. Birch, *Phys. Rev.* 71, 809–824 (1947).
- [6] W. B. Holzapfel, *Z. Kristallogr.* 216, 473–488 (2001).
- [7] T. Loerting, M. Bauer, I. Kohl, K. Watschinger, K. Winkel, and E. Mayer, *J. Phys. Chem. B* 115, 14167–14175 (2011).
- [8] M. Chaplin, *Water Phase Diagram*, http://www1.lsbu.ac.uk/water/water_phase_diagram.html accessed on April 28, 2015.
- [9] H. R. Pruppacher and J. D. Klett, *Microphysics of Clouds and Precipitation*. Dordrecht, 1980.
- [10] M. Seidl, K. Amann-Winkel, P. H. Handle, G. Zifferer, and T. Loerting, *Phys. Rev. B* 88, 174105 (2013).

- [11] O. Mishima, *Proc. Jpn. Acad., Ser. B* 86, 165–175 (2010).
- [12] P. H. Poole, F. Sciortino, U. Essmann, and H. E. Stanley, *Nature* 360, 324–328 (1992).
- [13] P. G. Debenedetti, *J. Phys.: Condens. Matter* 15, R1669–R1726 (2003).
- [14] O. Mishima, *PVT Phase Diagram of Liquid Water*, http://www.nims.go.jp/water/L_water_pvt.html accessed on April 28, 2015.
- [15] D. T. Limmer and D. Chandler, *J. Chem. Phys.* 135, 134503 (2011).
- [16] D. T. Limmer and D. Chandler, *J. Chem. Phys.* 138, 214504 (2013).
- [17] M. Seidl, K. Amann-Winkel, J. Bernard, and T. Loerting, *Nachr. Chem.* 63, 111–115 (2015).
- [18] T. Loerting, K. Winkel, M. Seidl, M. Bauer, C. Mitterdorfer, P. H. Handle, C. G. Salzmann, E. Mayer, J. L. Finney, and D. T. Bowron, *Phys. Chem. Chem. Phys.* 13, 8783–8794 (2011).
- [19] C. G. Salzmann, P. G. Radaelli, B. Slater, and J. L. Finney, *Phys. Chem. Chem. Phys.* 13, 18468–18480 (2011).
- [20] V. Fuentes-Landete, C. Mitterdorfer, P. H. Handle, G. N. Ruiz, J. Bernard, A. Bogdan, M. Seidl, K. Amann-Winkel, J. Stern, S. Fuhrmann, and T. Loerting, in P. G. Debenedetti, M. A. Ricci, and F. Bruni (Eds.), *Proceedings of the International School of Physics “Enrico Fermi”, Volume 187: Water: Fundamentals as the Basis for Understanding the Environment and Promoting Technology*. Amsterdam, 2015, 173–208.
- [21] O. Mishima, L. D. Calvert, and E. Whalley, *Nature* 310, 393–395 (1984).
- [22] I. Kohl, E. Mayer, and A. Hallbrucker, *Phys. Chem. Chem. Phys.* 3, 602–605 (2001).
- [23] C. G. Salzmann, T. Loerting, S. Klotz, P. W. Mirwald, A. Hallbrucker, and E. Mayer, *Phys. Chem. Chem. Phys.* 8, 386–397 (2006).
- [24] M. Bauer, M. S. Elsaesser, K. Winkel, E. Mayer, and T. Loerting, *Phys. Rev. B* 77, 220105 (2008).
- [25] M. Bauer, K. Winkel, D. M. Toebbens, E. Mayer, and T. Loerting, *J. Chem. Phys.* 131, 224514 (2009).
- [26] C. G. Salzmann, E. Mayer, and A. Hallbrucker, *Phys. Chem. Chem. Phys.* 6, 5156–5165 (2004).
- [27] M. Seidl, M. S. Elsaesser, K. Winkel, G. Zifferer, E. Mayer, and T. Loerting, *Phys. Rev. B* 83, 100201 (2011).
- [28] T. Loerting, C. Salzmann, I. Kohl, E. Mayer, and A. Hallbrucker, *Phys. Chem. Chem. Phys.* 3, 5355–5357 (2001).
- [29] K. Winkel, M. S. Elsaesser, E. Mayer, and T. Loerting, *J. Chem. Phys.* 128, 044510 (2008).
- [30] K. Winkel, M. S. Elsaesser, M. Seidl, M. Bauer, E. Mayer, and T. Loerting, *J. Phys. Cond. Matt.* 20, 494212 (2008).
- [31] K. Winkel, E. Mayer, and T. Loerting, *J. Phys. Chem. B* 115, 14141–14148 (2011).
- [32] O. Mishima, L. D. Calvert, and E. Whalley, *Nature* 314, 76–78 (1985).
- [33] M. Seidl, A. Fayter, J. N. Stern, G. Zifferer, and T. Loerting, *Phys. Rev. B* 91, 144201 (2015).
- [34] P. H. Handle, M. Seidl, and T. Loerting, *Phys. Rev. Lett.* 108, 225901 (2012).
- [35] M. S. Elsaesser, K. Winkel, E. Mayer, and T. Loerting, *Phys. Chem. Chem. Phys.* 12, 708–712 (2010).

- [36] K. Winkel, D. T. Bowron, T. Loerting, E. Mayer, and J. L. Finney, *J. Chem. Phys.* **130**, 204502 (2009).
- [37] G. P. Johari, *J. Chem. Edu.* **51**, 23–27 (1974).
- [38] M. D. Ediger, C. A. Angell, and S. R. Nagel, *J. Phys. Chem.* **100**, 13200–13212 (1996).
- [39] A. Cavagna, *Phys. Rep.* **476**, 51–124 (2009).
- [40] C. A. Angell, *Annu. Rev. Phys. Chem.* **55**, 559–583 (2004).
- [41] T. Loerting, V. V. Brazhkin, and T. Morishita, in S. A. Rice (Ed.), *Advances in Chemical Physics: Volume 143*. Hoboken, New Jersey, 2009, 29–82.
- [42] H. E. Stanley (Ed.), *Advances in Chemical Physics: Volume 152: Liquid Polymorphism*. Hoboken, New Jersey, 2013.
- [43] N. Giovambattista, in H. E. Stanley (Ed.), *Advances in Chemical Physics: Volume 152: Liquid Polymorphism*. Hoboken, New Jersey, 2013, 113–138.
- [44] J. J. Shephard, J. S. O. Evans, and C. G. Salzmann, *J. Phys. Chem. Lett.* **4**, 3672–3676 (2013).
- [45] T. Loerting, V. Fuentes-Landete, P. H. Handle, M. Seidl, K. Amann-Winkel, C. Gainaru, and R. Böhmer, *J. Non-Cryst. Solids* **407**, 423–430 (2015).
- [46] M. S. Elsaesser, I. Kohl, E. Mayer, and T. Loerting, *J. Phys. Chem. B* **111**, 8038–8044 (2007).
- [47] K. Winkel, W. Schustereder, I. Kohl, C. G. Salzmann, E. Mayer, and T. Loerting, in W. F. Kuhs (Ed.), *Physics and Chemistry of Ice*. Cambridge, 2007, 641–648.
- [48] C. R. Bina and A. Navrotsky, *Nature* **408**, 844–847 (2000).
- [49] J. Leliwa-Kopystynski, *Adv. Space Res.* **15**, 69–78 (1995).
- [50] P. Ehrenfreund, H. J. Fraser, J. Blum, J. H. E. Cartwright, J. M. Garcia-Ruiz, E. Hadamcik, A. C. Levasseur-Regourd, S. Price, F. Prodi, and A. Sarkissian, *Planet. Space Sci.* **51**, 473–494 (2003).
- [51] H. Tanaka, *Eur. Phys. J. E* **35**, 113 (2012).